Doping effects of multiferroic manganites $YMn_{0.9}X_{0.1}O_3$ (X=Al, Ru, and Zn)

Junghwan Park, Misun Kang, Jiyeon Kim, Seongsu Lee,* Kwang-Hyun Jang, A. Pirogov, and J.-G. Park†
Department of Physics, SungKyunKwan University, Suwon 440-746, Korea

Changhee Lee
Neutron Science Division, Korea Atomic Energy Research Institute, Daejon 305-353, Korea

S.-H. Park and Hyoung Chan Kim
National Fusion Research Institute, Daejeon 305-333, Korea

(Received 23 July 2008; revised manuscript received 28 January 2009; published 25 February 2009)

In order to understand the unusual magnetic phase of multiferroic hexagonal manganites, we have investigated the doping effects of hexagonal manganites $YMn_{0.9}X_{0.1}O_3$ (X=Al, Ru, and Zn) by using bulk measurements as well as neutron-diffraction experiments. We have also re-examined the magnetic structure of $YMnO_3$ to find that it has mainly the Γ_3 representation with an about 18% mixing of the Γ_4 representation. Upon doping nonmagnetic atoms such as Al, Ru, and Zn at the Mn site, the mixing of the two representations gets increased with an angle growing between the magnetic moment and the crystallographic a axis (ϕ); for example, ϕ changes from 10° for $YMnO_3$ to 45° for $YMn_{0.9}Zn_{0.1}O_3$. At the same time, the ordered moment becomes significantly reduced with doping, while the transition temperature is suppressed slightly.

DOI: 10.1103/PhysRevB.79.064417 PACS number(s): 75.25.+z, 75.40.Cx, 75.50.Ee

I. INTRODUCTION

There has been renewed interest in materials that exhibit both ferroelectric and magnetic transitions.[1] These so-called multiferroic systems offer rare opportunities where the two seemingly independent phenomena are coupled to one another, and so we can explore the unusual coupling of the two effects mostly heavily utilized in modern technologies.

The hexagonal manganites $RMnO_3$ are one such rare example of the multiferroic materials with the coexistence of both ferroelectric and antiferromagnetic transitions. For example, $YMnO_3$ shows an antiferromagnetic transition at T_N =75 K and a ferroelectric transition at T_C=913 K.[2] Therefore, the hexagonal manganites offer a unique window of opportunities of exploring a possible coupling between the two order parameters. In fact, these hexagonal manganites have been extensively investigated over the past few years and are the first real examples of multiferroic materials with a convincing demonstration of such a desirable coupling between ferroelectricity and magnetism.[3]

$RMnO_3$ forms in the hexagonal manganites with space group $P6_3cm$ for rare-earth elements with a relatively small ionic radius, e.g., Ho, Er, Tm, Yb, Lu, Y, and Sc, while another $RMnO_3$ manganite of an orthorhombic structure with space group *Pnma* is favorable for rare-earth elements with a relatively large ionic radius, e.g., La, Pr, Nd, Sm, Eu, Gd, Tb, and Dy.[4]

Of further interest is that the Mn ions of the hexagonal manganites form a natural two-dimensional (2D) edge-sharing triangular network with a clear sign of magnetic frustration. What distinguishes $YMnO_3$ from other well-documented 2D spin systems is that it is a geometrically frustrated system with natural 2D Heisenberg spin. Our neutron-scattering studies indeed revealed that $YMnO_3$ exhibits clear diffuse scattering even well above T_N.[5] In the antiferromagnetic phase, the ordered moments lie in the basal plane with a value of $3.30\mu_B$ per Mn atom, reduced from the ionic value of $4.0\mu_B$ for Mn^{3+}. This microscopic evidence of magnetic frustration is consistent with bulk properties. For example, the antiferromagnetic ordering temperature of $YMnO_3$ (T_N=75 K) is much suppressed when compared with its Curie-Weiss temperature θ_{CW}=−545 K. Therefore, the ratio of $f=|\theta_{CW}|/T_N$ is as large as 7.3 for $YMnO_3$, which makes it one of the so-called geometrically frustrated systems.[6]

In regard to the experimental observations, one should also discuss the magnetic structure of the hexagonal manganites. Although altogether six different representations are possible with $\vec{k}=0$ according to magnetic group theories,[7] only four one-dimensional (1D) representations seem to be particularly favorable among all the hexagonal manganites known to date. For example, the magnetic peaks of $YMnO_3$ can be explained by either Γ_1 or Γ_3 representations while those of $ErMnO_3$ are compatible with Γ_2 or Γ_4 representations. Interestingly these magnetic ground states can be changed from one to another continuously by doping at the rare-earth site[8] or external pressure.[9] For example, our studies[8] of $Er_{1-x}Y_xMnO_3$ demonstrated that the magnetic structure changes gradually from the Γ_1/Γ_3 representation of $YMnO_3$ to the Γ_2/Γ_4 representation of $ErMnO_3$ while the ordered moment remains almost unchanged in magnitude over the entire doping range. Similar changes in the magnetic structure were observed for both $YMnO_3$ and $LuMnO_3$ in the pressure range of 6 GPa.[9] Furthermore, it was recently suggested that even pure hexagonal manganites such as $YMnO_3$ might have a mixed magnetic structure with a mixing coefficient of 0.19,[10] Γ_1/Γ_3 and Γ_2/Γ_4.

With such a subtle nature of the magnetic ground state of hexagonal $RMnO_3$, naturally it is interesting to further investigate how the ground state responds to various perturbations. One probably mostly *brute force* and, at the same time, revealing perturbation is doping at the Mn site, where all the actions take place. Because of the natural 2D triangular net-

TABLE I. Summary of the refinement results of neutron-diffraction data taken at 300 K for $YMn_{0.9}X_{0.1}O_3$. We refined the data using the space group $P6_3cm$.

	Crystal parameters			Agreement factors		
X atoms	a (Å)	c (Å)	V (Å^3)	R_p (%)	R_{wp} (%)	χ^2
$YMnO_3$	6.1392(1)	11.3913(2)	372.28(1)	4.67	6.26	1.72
Al	6.1382(1)	11.3720(2)	371.06(1)	3.68	5.00	1.99
Ru	6.1489(1)	11.4057(2)	373.46(1)	3.21	4.26	1.58
Zn	6.1639(1)	11.3802(2)	374.44(1)	3.02	3.90	2.12

work of the Mn moments, it is an intriguing question to ask what kind of new states may emerge out of the frustrated state as sometimes observed in other geometrically frustrated magnetic systems.[6] If successful, such new emergent states will shed important light on the exciting ground state of the hexagonal $RMnO_3$.

In order to explore such possibilities and, at the same time, understand the subtle nature of the magnetic structure, we have undertaken studies of Mn-site doping experiments. With a different suggestion[10] about the mixing magnetic structure even for pure hexagonal manganites, we have also reanalyzed our neutron-diffraction data of $YMnO_3$.

II. EXPERIMENTAL DETAILS

We have prepared several Mn-site doped samples by nonmagnetic elements such as Al, Ru, and Zn using Y_2O_3, Mn_2O_3, Al_2O_3, Ru_2O_3, and ZnO of 99.999% purity [analytical reagent (AR) grade] by a standard solid-state reaction method. All the starting materials were mixed and ground several times in order to produce a homogeneous mixture. The final sintering was made at 1300 °C for 24 h with intermediate grinding. Subsequent x-ray diffraction (XRD) measurements with D/MAX-2200 Ultima (Rigaku) using Cu $K\alpha$ showed that only $YMn_{0.9}X_{0.1}O_3$ (X=Al, Ru, and Zn) have no trace of impurity phases, and their measured patterns can be indexed according to the $P6_3cm$ space group of the hexagonal manganites. We also measured magnetization using a commercial superconducting quantum interference device (SQUID) magnetometer (MPMS-5XL, Quantum Design) from 2 to 300 K and a vibrating sample magnetometer (VSM) (Lakeshore 735) from 300 to 600 K. Heat capacity was measured from 2 to 250 K using a commercial cryostat (PPMS9, Quantum Design). Neutron-diffraction measurements were also carried out from 10 to 300 K with a wavelength of λ=1.835 Å using a high-resolution powder diffractometer (HRPD) at the Korea Atomic Energy Research Institute. All the diffraction data were analyzed using the FULLPROF program.[11] We note that although we undertook neutron-diffraction experiments of the three doped samples for this work, we also used the neutron-diffraction data of $YMnO_3$ for the reanalysis that had previously been reported by us in Ref. 5.

III. RESULTS AND ANALYSIS

Table I is the summary of our refinement results of neutron-diffraction data taken at 300 K for $YMn_{0.9}X_{0.1}O_3$. As one can see, all the samples have the space group $P6_3cm$ of the hexagonal structure. The overall agreement factors of the refinements are better than χ^2=2.12, R_p=4.67%, and R_{wp}=6.26% for all the four samples. By examining the XRD patterns of samples with several other doping concentrations, we found that no single phase exists for more than 10% of nominal doping concentration. It is also to be noted that the lattice constants and the unit-cell volume of the doped samples change in accordance with the ionic radius of the dopant atoms with the unit-cell volume increasing from Al to Zn. A noteworthy point is that unlike other ions Zn has 2+ valence so doping of Zn at the Mn^{3+} site will not only induce chemical pressure effect but also change the valence of Mn ions from 3+ toward a mixed-valence state.

Similarly gradual doping effects have been observed in our subsequent magnetization measurements (see Fig. 1). Similar to the undoped parent $YMnO_3$ all the doped samples do not exhibit a clear anomaly at the expected transition temperatures. Instead, we observed that Curie-Weiss temperature (θ_{CW}) and the estimated effective moment (μ_{eff})

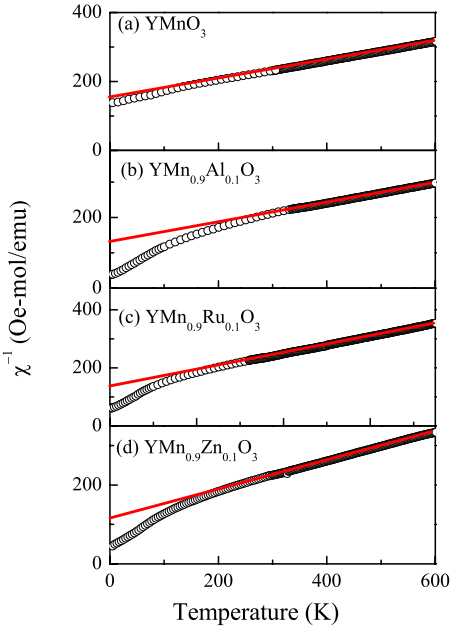

FIG. 1. (Color online) The temperature dependence of the inverse susceptibility is shown for three doped samples of $YMn_{0.9}X_{0.1}O_3$ (X=Al, Ru, and Zn) and $YMnO_3$. Symbols are for data point and the line is a fitting result using the Curie-Weiss law.

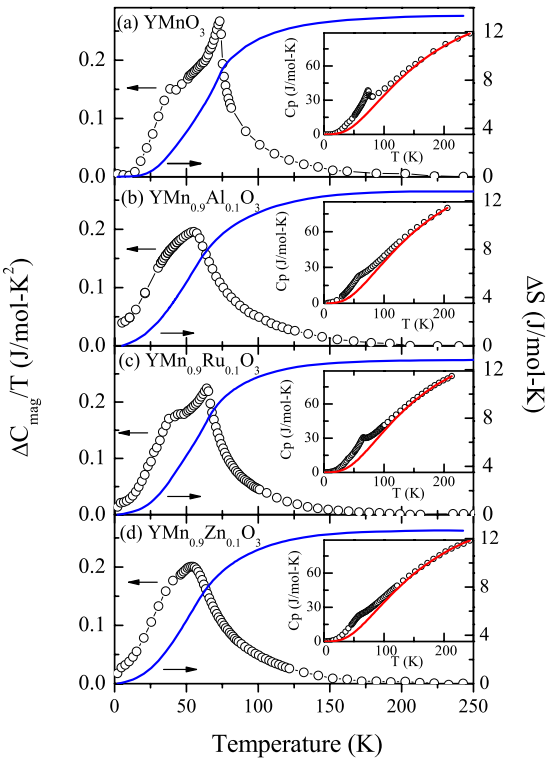

FIG. 2. (Color online) The temperature dependence of $\Delta C_{\mathrm{mag}}/T$ is shown for four samples after subtraction of phonon contributions. Lines in the main figures represent the magnetic entropy (ΔS). Inset figures in each main figure show the raw data of the specific heat (symbol) and the respective phonon estimate (lines) using Debye temperatures as discussed in text.

display a somewhat gradual change upon doping. For example, the Curie-Weiss temperatures are found to decrease with doping from $\theta_{\mathrm{CW}}=-526$ K ($YMnO_3$) to -446 K ($YMn_{0.9}Al_{0.1}O_3$), -421 K ($YMn_{0.9}Ru_{0.1}O_3$), and -388 K ($YMn_{0.9}Zn_{0.1}O_3$). Simultaneously, the effective moment (μ_{eff}) also shows a similar trend: $\mu_{\mathrm{eff}}=5.1\mu_B$ is estimated for $YMnO_3$ while it becomes 4.79, 4.71, and $4.64\mu_B$ for $YMn_{0.9}Al_{0.1}O_3$, $YMn_{0.9}Ru_{0.1}O_3$, and $YMn_{0.9}Zn_{0.1}O_3$, respectively. The fact that the Zn-doped sample shows the smallest μ_{eff} value is also consistent with the hole doping effect of Zn.

As further studies of the thermodynamic properties of the doped sample, we measured the heat capacity of all samples from 2 to 250 K. The raw data shown in the inset of Fig. 2 display a clear peak indicative of the antiferromagnetic transition. T_N as determined from the peak position in the heat-capacity data changes from 75 K for $YMnO_3$ to 70 K for $YMn_{0.9}Zn_{0.1}O_3$. We also plotted the magnetic specific heat $\Delta C_{\mathrm{mag}}/T$ in Fig. 2 after subtracting off phonon contributions. In order to calculate magnetic entropy from the heat-capacity data, we have estimated the phonon contribution (line in the inset) using the Debye model with two Debye temperatures. For $YMnO_3$ we used $\theta_1=413\pm5$ K and $\theta_2=805\pm6$ K that are similar to the reported values,[12] while we took the following values for the doped samples: $\theta_1=406\pm5$ K and $\theta_2=807\pm6$ K for $YMn_{0.9}Al_{0.1}O_3$, $\theta_1=398\pm5$ K and $\theta_2=766\pm6$ K for $YMn_{0.9}Ru_{0.1}O_3$, and $\theta_1=407\pm5$ K and $\theta_2=815\pm6$ K for $YMn_{0.9}Zn_{0.1}O_3$. This model with two Debye temperatures can be rationalized by the fact that there are two kinds of elements in our samples—three relatively heavy elements of Y, Al, Ru, Zn, and Mn and a relatively light element of O, which are expected to give rise to two distinctive Debye temperatures. By subtracting off the phonon contribution from the raw data, we have obtained the total magnetic entropy of 12.8 J/mol K for $YMn_{0.9}Al_{0.1}O_3$, 12.8 J/mol K for $YMn_{0.9}Ru_{0.1}O_3$, and 12.7 J/mol K for $YMn_{0.9}Zn_{0.1}O_3$ at 250 K (the lines in the main figures of Fig. 2). For comparison, the total magnetic entropy of the undoped $YMnO_3$ is 13.3 J/mol K at 250 K, which is very close to the theoretical magnetic entropy of 13.4 J/mol K. We can easily ascribe the decreased magnetic entropy to the reduced Mn concentration in the doped sample within the resolutions of our experiments.

As we noted previously, the triangular network of the Mn moments is generically frustrated with antiferromagnetic interaction as in $YMnO_3$. One such evidence can be found in the heat capacity such that as much as 1/3 of the total magnetic entropy is released above T_N for $YMnO_3$. Likewise, the doped samples also show that a similarly large part of the magnetic entropy is consumed above the actual magnetic transition temperature, i.e., experimental evidence of the magnetic frustration. One noteworthy point, however, is that the doped samples show relatively smaller entropy to be released above T_N than in $YMnO_3$ so they appear to be relatively less frustrated. This experimental observation is also consistent with the magnetic-susceptibility data. For example, we can define the usual frustration factor as the ratio between T_N and θ_{CW}, $f(=|\theta_{\mathrm{CW}}|/T_N)$, using the specific heat and inverse susceptibility data. Then the determined frustration factor is found to decrease with doping; it is $f=7.0$ for $YMnO_3$ while it becomes 6.2 for $YMn_{0.9}Al_{0.1}O_3$, 5.9 for $YMn_{0.9}Ru_{0.1}O_3$, and 5.5 for $YMn_{0.9}Zn_{0.1}O_3$.

How is this change in the bulk properties related to microscopic properties? In order to answer this question directly, we have investigated the magnetic structure of all the samples using the neutron powder-diffraction technique. Before presenting our results on the doped samples, let us discuss the results of the pure $YMnO_3$ first. In the light of recent polarized neutron-diffraction studies by Brown and Chatterji,[10] we think that it is timely to re-examine the powder data of $YMnO_3$. In our previous studies[5,13] of $YMnO_3$, we interpreted the magnetic structure as belonging to either Γ_1 or Γ_3 representation. However, the recent study[10] found that the magnetic structure even for pure $YMnO_3$ can have either mixed ($\Gamma_1+\Gamma_2$) or ($\Gamma_3+\Gamma_4$) representations. This work prompted us to reanalyze our data using the four types of magnetic structure as shown in Fig. 1 of Ref. 10. As we have summarized in Table II, although the four models have very similar agreement factors to one another, the two mixed structures are found to be more favorable over the unmixed structures. Moreover, the mixed structure of ($\Gamma_3+\Gamma_4$) has marginally lower agreement factors than the other mixed structure of ($\Gamma_1+\Gamma_2$). Here we note that the observation of the second-harmonic signal for $YMnO_3$ with k parallel to the z axis is not consistent with the ($\Gamma_1+\Gamma_2$) structure since such a signal is not symmetrically allowed for the latter model.[14] So when combining both neutron-diffraction data and the

TABLE II. Summary of refinement results using the magnetic structure model of $YMnO_3$ with four one-dimensional irreducible representations.

Magnetic structure	Moment (μ_B/Mn)	ϕ (deg)	χ^2	R_{Bragg} (%)	R_p (%)	R_{mag} (%)
Γ_1	3.35(3)	90.0	3.12	2.13	6.25	6.22
Γ_3	3.32(2)	0.0	3.13	2.07	6.28	5.90
$\Gamma_1+\Gamma_2$	3.34(2)	80.8(1.0)	3.10	2.10	6.23	5.69
$\Gamma_3+\Gamma_4$	3.32(2)	10.3(1.2)	3.10	2.07	6.24	5.31

second-harmonic experiment, we can maintain that the mixed structure of $(\Gamma_3+\Gamma_4)$ is a true ground state for $YMnO_3$. In passing, we note that other combinations, $(\Gamma_1+\Gamma_4)$ and $(\Gamma_2+\Gamma_3)$, give rise to a similar value of agreement factors. However, these two mixed structures produce magnetic structures with Mn atoms at $z=0$ and 1/2 planes having different ordered moments, which we think is unrealistic.

With this conclusion, we then proceed to examine the tilting angle (ϕ) dependence of the $\Gamma_3+\Gamma_4$ structure. For that, we have specifically investigated the ϕ dependence of the magnetic structure (see Fig. 3); ϕ is the angle between the a axis and the Mn moment. As seen in Fig. 3, the agreement factor has the lowest value for $\phi=10.3°$, supporting the conclusion of Ref. 10. With this information, we then continued to analyze the neutron-diffraction data taken on doped samples. First of all, the evolution of the magnetic structure upon doping can be readily seen even in the raw data taken at 10 K. As shown in Fig. 4(a), the (1 0 0) Bragg peak is a pure magnetic peak and totally absent for the Γ_4 representation while another pure magnetic peak of (1 0 1) is seen for both Γ_3 and Γ_4 representations. As one can see in the figure, the ratio of the intensity of the two magnetic peaks varies with doping. This change in the ratio can be explained by the change in a mixing ratio between the Γ_3 and Γ_4 representations. Following our conclusion of the magnetic structure of $YMnO_3$ as discussed above, we analyzed the data of the doped samples using the mixed structure of the Γ_3 and Γ_4 representations from the beginning [see the magnetic structure shown in the inset of Fig. 4(a)].

Typical refinements of some representative results taken at 10 K are shown in Fig. 5 for four samples together with that of $YMnO_3$. During the refinement, we achieved reasonable agreement factors for all our fittings; the summary of the refinement results is given in Table III. We note that a model with the mixed Γ_1 and Γ_2 representations is found to have slightly worse agreement factors for all the doped samples. In Fig. 4(b), we plot the total magnetic moment as a function of temperature, which was obtained from the refinement. As one can see in Fig. 4(b), the Mn moment decreases with doping from $3.32\mu_B$/Mn atom for $YMnO_3$ to $3.04\mu_B$/Mn atom for $YMn_{0.9}Al_{0.1}O_3$, to $3.06\mu_B$/Mn atom for $YMn_{0.9}Ru_{0.1}O_3$, and to $2.53\mu_B$/Mn atom for $YMn_{0.9}Zn_{0.1}O_3$ at 10 K. As Mn is in a 3+ valence state for $YMnO_3$, $YMn_{0.9}Al_{0.1}O_3$, and $YMn_{0.9}Ru_{0.1}O_3$, it is expected to have a full spin moment of $4\mu_B$ under the assumption that the orbital moment is completely quenched. On the other hand, Mn ions of $YMn_{0.9}Zn_{0.1}O_3$ has both 3+ and 4+ valence states since Zn has 2+ valence unlike Mn, Al, and Ru, having 3+ valence, so the expected full spin moment is $3.9\mu_B$/Mn atom for the 10% Zn-doped sample. Thus the rather drastic reduction in the magnetic moment for the Zn-doped sample is striking but not totally unexpected when compared with the results of the other two doped samples. This, together with the general tendency of the reduction in the moment with doping, points to an intriguing possibility about the nature of the magnetic ground states. As we noted, the ordered state of the undoped $YMnO_3$ exhibits characteristic features of frustrated magnetic systems. For such frustrated magnetic sys-

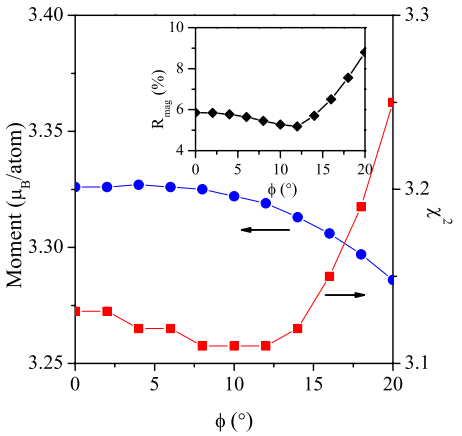

FIG. 3. (Color online) Using a mixed $\Gamma_3+\Gamma_4$ structure with ϕ angle as a variable, we refined our results to obtain moment and χ^2 as shown in the main figure and R_{mag} agreement factor in the inset. From this result, we can conclude that the correct magnetic structure of $YMnO_3$ has $\phi=10°$.

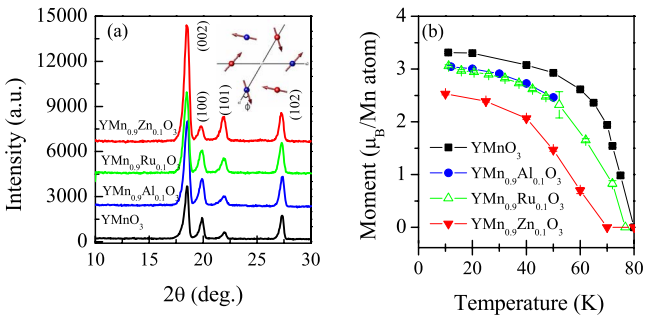

FIG. 4. (Color online) (a) Neutron-diffraction patterns taken at 10 K with the data shifted upward for better presentation. The inset in (a) shows the magnetic structure we used for the analysis and (b) displays the temperature dependence of the ordered magnetic moment of Mn.

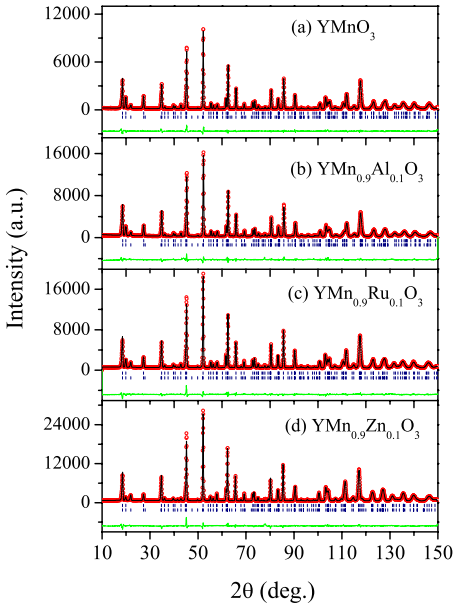

FIG. 5. (Color online) Observed (circle) and calculated (line) neutron-diffraction patterns for four samples taken at 10 K. In order to refine the data, we used the space group $P6_3cm$ and a mixed $\Gamma_3+\Gamma_4$ representation. The lines at the bottom of each figure are the difference curves between the observed and calculated diffraction patterns. The bars indicate the position of the nuclear (upper) and magnetic (lower) Bragg peaks.

tems, doping is often regarded as a way of relieving the degeneracy of frustrated states through a so-called order-by-disorder mechanism.[6] Therefore, the fact that the magnetic moment of $YMnO_3$ is reduced with doping seems to be at variance with the order-by-disorder mechanism. Moreover, the fact that we have seen the biggest drop in the moment for the Zn-doped sample indicates that having Mn^{3+} is rather important for the formation of the magnetic ground state.

Another interesting point is the doping effect on T_N variations. As shown in Fig. 4(b) and summarized in Table III, the ordering temperature is reduced progressively with doping compared with $YMnO_3$. In order to explain the measured T_N variation, we should consider effects of doping. Doping ions with different ionic radius will inevitably change the lattice constant and also the Mn-Mn bond distance. This change in the Mn-Mn bond distance, in particular on the *ab* plane, leads naturally to variations in the exchange integral, which is a critical parameter for the formation of the magnetic ground state. Second, by doping nonmagnetic elements at the Mn site we break the exchange paths. This broken exchange path will also make a magnetic state less stable. With these two considerations in mind, we can examine our experimental results. As summarized in Table III, the *a*-axis lattice constant clearly increases with doping, except for the case of the Al doping. It is particularly noticeable that the Zn-doped sample has a distinctively larger *a*-axis lattice constant compared with the other two doped samples. If we think of this variation in terms of a Mn-Mn bond distance, then it corresponds roughly to about 0.6% of a relative change in the Mn-Mn bond distance compared with $YMnO_3$. This then would give rise roughly to a decrease of about 4% in the exchange integral J (Ref. 15) and also a similar drop in T_N. This theoretical anticipation appears to be consistent with our experimental results. For example, the Zn-doped sample with the largest Mn-Mn bond distance shows the biggest drop in T_N. We also note that an opposite effect, i.e., an increase in T_N due to a shorter Mn-Mn bond distance, has been reported in our high-pressure experiments.[16]

Further doping effect on the magnetic ground state can be seen in the magnetic structure. As we discussed before, the magnetic structure of $YMnO_3$ has a mixed $\Gamma_3+\Gamma_4$ structure with a mixing angle of $\phi=10°$. Upon doping, this angle ϕ increases to 45° for the Zn-doped sample (see Table III). Again, the biggest change is seen for the Zn-doped sample that is consistent with our other experimental observations of the magnetic ground state.

IV. DISCUSSION

Although not an ideal probe, nevertheless doping experiments often provide a rare window to otherwise elusive features of the system under investigation. In our case, primarily, doping has two main direct effects: one is a chemical pressure effect and the other a hole doping effect. The chemical pressure effect is complementary to the real pressure studies. Through doping, we found that the magnetic ground states evolve progressively from a much frustrated state to one with less frustration and, at the same time, with lower transition temperatures and magnetic structures different from that of pure $YMnO_3$. These experimental observations, in particular variations in T_N, are consistent with doping-induced Mn-Mn bond distances. In fact, we have recently pointed out that this Mn-Mn bond distance, more importantly its temperature dependence, is a key to the desirable multi-

TABLE III. Summary of the refinement results of neutron powder-diffraction patterns taken at 10 K. For our analysis, we used the space group of $P6_3cm$ and the magnetic structure of a mixed $(\Gamma_3+\Gamma_4)$ representation as discussed in the text. T_N was determined from the heat-capacity data shown in Fig. 2.

X atom	a (Å)	c (Å)	V (Å^3)	Mn-Mn bond distance (Å)	Moment (μ_B/Mn)	ϕ (deg)	T_N (K)
$YMnO_3$	6.1205(1)	11.4012(3)	369.88(1)	3.527(8)	3.32(2)	10.3(1.2)	75
Al	6.1202(3)	11.3826(5)	369.24(3)	3.533(5)	3.04(2)	14.2(1.1)	73
Ru	6.1281(1)	11.4112(3)	371.12(1)	3.538(8)	3.06(2)	25.3(0.7)	73
Zn	6.1451(1)	11.3881(2)	372.42(1)	3.548(5)	2.53(2)	44.5(0.7)	70

ferroic behavior of $YMnO_3$.[17] One can imagine that different Mn-Mn bond distances with different exchange integrals lead to different magnetic ground states and modifications to thermodynamic properties as we have observed in our studies. Therefore, our doping experiment also supports the conclusion that a spin-lattice coupling via the Mn-Mn bond is essential in understanding the magnetic ground states, structure, and thermodynamic properties of multiferroic $YMnO_3$. Although we consider it as a very remote possibility, we should note that some inhomogeneous models such as phase separation seen in doped orthorhombic manganites can, in principle, be a plausible explanation for our observation for the doped materials.

To summarize, we have found that Al, Ru, and Zn doping at the Mn site of $YMnO_3$ significantly modifies the magnetic properties of the Mn triangular network. Most of our experimental findings can be understood in terms of the doping-induced change in the Mn-Mn bond distance.

ACKNOWLEDGMENTS

We acknowledge S. V. Streltsov for helpful comments in Ref. 15. Works at SungKyunKwan University were supported by the Korea Research Foundation (Grant No. KRF-2005-015-C00153), the 21st Century Frontier R&D Program for Hydrogen Energy, and the KOSEF through the Acceleration Research Program (Grant No. R17-2008-033-01000-0).

*Present address: Neutron Science Division, Korea Atomic Energy Research Institute, Daejon 305-353, Korea.
†jgpark@skku.edu

[1] W. Eerenstein, N. D. Mathur, and J. F. Schott, Nature (London) **442**, 759 (2006); S.-W. Cheong and M. Mostovoy, Nature Mater. **6**, 13 (2007).
[2] I. G. Ismailzade and S. A. Kizhaev, Sov. Phys. Solid State **8**, 236 (1965); G. Smolenskii and I. Chupis, Sov. Phys. Usp. **25**, 475 (1982).
[3] Th. Lottermoser, Th. Lonkai, U. Amann, D. Hohlwein, J. Ihringer, and M. Fiebig, Nature (London) **430**, 541 (2004).
[4] M. A. Gilleo, Acta Crystallogr. **10**, 161 (1957); H. Yakel Jr., W. C. Koehler, E. F. Bertaut, and E. F. Forrat, *ibid.* **16**, 957 (1963).
[5] Junghwan Park, J.-G. Park, Gun Sang Jeon, Han-Yong Choi, Changhee Lee, W. Jo, R. Bewley, K. A. McEwen, and T. G. Perring, Phys. Rev. B **68**, 104426 (2003).
[6] A. P. Ramirez, in *Handbook of Magnetic Materials*, edited by K. H. J. Buschow (North-Holland, Amsterdam, 2001), Vol. 13.
[7] A. Munoz, J. A. Alonso, M. J. Martinez-Lope, M. T. Casais, J. L. Martinez, and M. T. Fernandez-Diaz, Phys. Rev. B **62**, 9498 (2000).
[8] M. Chandra Sekhar, S. Lee, G. Choi, C. Lee, and J.-G. Park, Phys. Rev. B **72**, 014402 (2005).
[9] D. P. Kozlenko, S. E. Kichanov, S. Lee, J.-G. Park, V. P. Glazkov, and B. N. Savenko, JETP Lett. **82**, 193 (2005).
[10] P. J. Brown and T. Chatterji, J. Phys.: Condens. Matter **18**, 10085 (2006).
[11] J. Rodríguez-Carvajal, Physica B **192**, 55 (1993).
[12] D. G. Tomuta, S. Ramakrishnan, G. J. Nieuwenhuys, and J. A. Mydosh, J. Phys.: Condens. Matter **13**, 4543 (2001).
[13] Seongsu Lee, A. Pirogov, Jung Hoon Han, J.-G. Park, A. Hoshikawa, and T. Kamiyama, Phys. Rev. B **71**, 180413(R) (2005).
[14] M. Fiebig, D. Fröhlich, K. Kohn, St. Leute, Th. Lottermoser, V. V. Pavlov, and R. V. Pisarev, Phys. Rev. Lett. **84**, 5620 (2000).
[15] According to Harrison parametrization, the exchange integral J is inversely proportional to a bond distance, $J \sim d^{-10}$; W. A. Harrison, *Elementary Electronic Structure* (World Scientific, Singapore, 1999).
[16] D. P. Kozlenko, S. E. Kichanov, S. Lee, J.-G. Park, and B. N. Savenko, J. Phys.: Condens. Matter **19**, 156228 (2007).
[17] Seongsu Lee, A. Pirogov, Misun Kang, Kwang-Hyun Jang, M. Yonemura, T. Kamiyama, S-W. Cheong, F. Gozzo, Namsoo Shin, H. Kimura, Y. Noda, and J.-G. Park, Nature (London) **451**, 805 (2008).